

Generation of χ^2 solitons from the Airy wave through the parametric instability

Thawatchai Mayteevarunyoo

*Department of Telecommunication Engineering,
Mahanakorn University of Technology, Bangkok 10530, Thailand*

Boris A. Malomed

*Department of Physical Electronics,
School of Electrical Engineering, Faculty of Engineering,
Tel Aviv University, Tel Aviv 69978, Israel*

Abstract

Spontaneous creation of solitons in quadratic media by the downconversion, i.e., parametric instability against the generation of fundamental-frequency excitations, from the truncated Airy-wave (AW) mode in the second-harmonic component is studied. Parameter regions are identified for the generation of one, two, and three solitons, with additional small-amplitude “jets”. Shares of the total power carried by individual solitons are found. Also considered are soliton patterns generated by the downconversion from a pair of AWs bending in opposite directions.

Transmission of waves with a specific intrinsic structure along curved paths has drawn a great deal of interest in photonics and related areas. A well-known class of self-bending beams is based on Airy wave (AW) packets, as demonstrated, theoretically and experimentally, in quantum mechanics [1], a variety of settings in optics [2]-[21], plasmonics [22]-[24], electron beams [25], Bose-Einstein condensates [26], gas discharge [27], and water waves [28]. While Airy beams are eigenmodes of linear media, their propagation in systems with cubic [9]-[21] and quadratic (alias $\chi^{(2)}$) [5]-[7], [14] nonlinearities was studied too. In the latter case, the formation of two-color beams by the AW input launched in the fundamental-frequency (FF) component (*upconversion*) was analyzed theoretically and demonstrated experimentally. The objective of the present work is to analyze an alternative possibility of the *downconversion*, i.e., the generation of solitons, that are fundamental eigenmodes of the $\chi^{(2)}$ media, by the parametric instability (PI) of (truncated) Airy beams launched in the second harmonic (SH), which are exact linear modes of the system if FF perturbations are not added. In this connection, it is relevant to note that formation (*shedding*) of solitons by AWs in cubic media was recently analyzed [10] and observed experimentally [28], while the formation of $\chi^{(2)}$ solitons via the PI of straight SH wave packets, such as symmetric Gaussians, was studied still earlier [29]-[31].

It should be stressed that the scenario of the generation of solitons by small random perturbations in the FF field interacting with the parametrically-unstable SH input itself demonstrates instability, producing quasi-random patterns including $\chi^{(2)}$ solitons and “jets” (see below). Nevertheless, systematic simulations make it possible to identify regular features of the emerging soliton sets, such as the number of major solitons and shares of the total power carried away by each of them.

The “type-I” model of the one-dimensional $\chi^{(2)}$ system, with the single FF component, u , and the SH component, w , is taken in the usual scaled form [29]-[31]:

$$\begin{aligned} iu_z &= -(1/2)u_{xx} - u^*w, \\ 2iw_z &= qw - (1/2)w_{xx} - (1/2)u^2, \end{aligned} \tag{1}$$

where z and x are the propagation distance and transverse coordinate, the second derivatives represent the diffraction in the paraxial approximation, $*$ stands for the complex conjugate, and the mismatch parameter, q , may be scaled to $q = +1, 0, -1$. The system conserves the

total power (Manley-Rowe invariant) and momentum,

$$P = \int_{-\infty}^{+\infty} (|u|^2 + 4|w|^2) dx, \quad M = i \int_{-\infty}^{+\infty} (u_x^* u + 2w_x^* w) dx, \quad (2)$$

along with the corresponding Hamiltonian.

The self-bending linear modes for the SH in the absence of the FF component are generated by the input in the form of truncated AWs [2],

$$w(x, z = 0) = W_0 \text{Ai}(\alpha x) \exp((\alpha/A)x), \quad u = 0, \quad (3)$$

where Ai is the standard Airy function, W_0 and $1/\alpha$ determine the amplitude and spatial scale of the wave, while the truncation parameter, A , makes the total power of input finite [2]:

$$P = P_0 \alpha^3 \sqrt{A/8\pi} \exp((2/3)A^{-2}), \quad P_0 \equiv W_0^2/\alpha^4. \quad (4)$$

Most results are displayed below for $A = 10$, in which case the multi-lobe structure of the truncated input seems virtually identical to the untruncated one. Note that, in the case of $q = 0$, which is chiefly considered here, the scaling invariance of Eqs. (1) demonstrates that, at fixed A , the normalized total power of different inputs is actually measured by single parameter P_0 defined in Eq. (4).

In simulations, input (3) was used for the SH field, with small (“seed”) random perturbations in the FF mode initiating the onset of the PI (the results do not essentially depend on characteristics of the seed). For collecting the results which are displayed below, it was necessary to use a large integration domain, of size $|x| \leq 2^{11}$. In the course of the simulations, it was checked that the total power is conserved, and the total momentum remains equal to zero, see Eq. (2).

As shown in the plots collected in the left column of Figs. 1 and 2, outcomes of the PI-initiated evolution can be summarized as the generation of one or several clearly identified $\chi^{(2)}$ solitons, supplemented by “jets” with essentially smaller amplitudes, and still smaller radiation features. Additional analysis demonstrates that the shape of individual solitons is very close to that known in the standard $\chi^{(2)}$ model [29]-[31]. It is seen that the number of the major solitons raises from 1 to 2 to 3, as P_0 increases from 3164 to 5294 to 30925. The generation of the patterns being initiated by random small perturbations amplified by the PI, the picture always includes random features, making it difficult to exactly identify values of P_0 corresponding to boundaries between the outcomes with different numbers of major

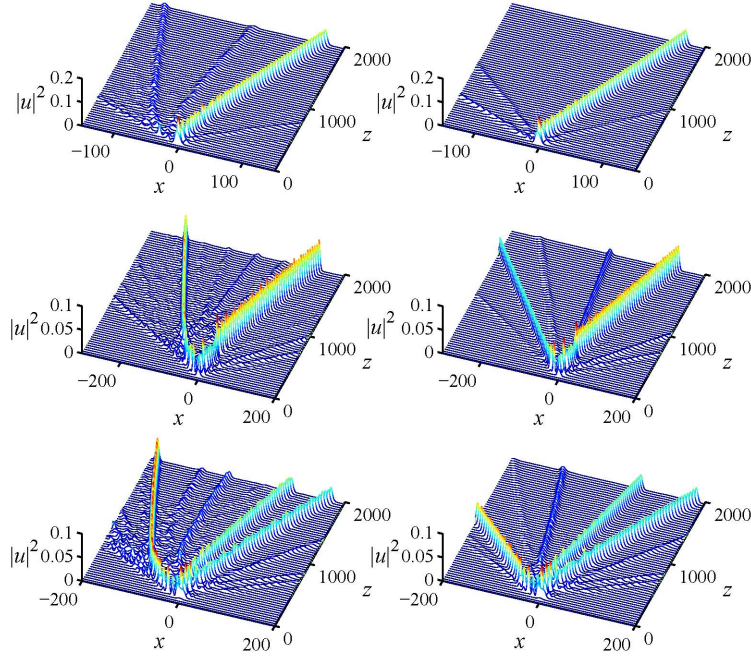


FIG. 1: (Color online) The top, middle, and bottom rows display the generation of patterns featuring 1, 2, and 3 major $\chi^{(2)}$ solitons, along with “jets”, from the SH input (3) with $W_0 = 0.2571, \alpha = 0.0855$; $W_0 = 0.2366, \alpha = 0.0570$; and $W_0 = 0.2057, \alpha = 0.0342$, respectively (in all cases, $A = 10$). Here (and in Fig. 4 below) the intensity of the FF component is displayed; the respective patterns of the SH field are shown in Figs. 2 and 5. To demonstrate how the coherence of the input affects the output, left and right panels display, severally, the results generated by the full AW input, and by its “tailless” version, in which all but the main lobe of the AW shape is cut off. This figure, as well as Figs. 3 and 4, 5, pertain to the system with zero mismatch, $q = 0$.

solitons. Nevertheless, the trend to the increase of the soliton number with the growth of P_0 is evident. Results demonstrating more than three major solitons are not presented here, as the respective simulations must be run in a huge domain, and they would require a very wide waveguide for the experimental realization.

If two or three solitons are generated by the AW input, their origin cannot be unambiguously linked to particular lobes in the Airy-wave input, as the emerging solitons become visible after some distance of “latent” growth of the PI, which separates the input and the multi-soliton pattern. Nevertheless, the generation of the multi-soliton pattern, along with the “jets”, is a coherent effect provided by the specific structure of the input. To further address the latter point, plots collected in the right column of Fig. 1 report the results of

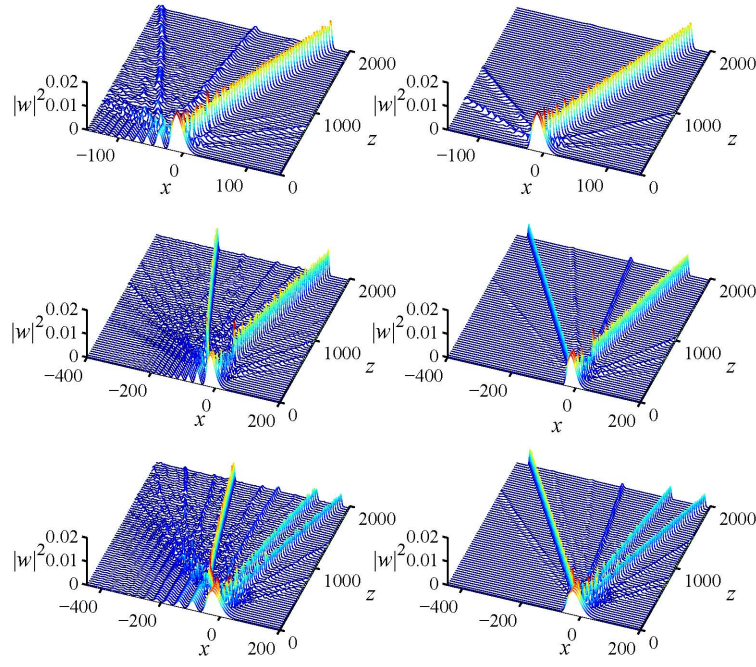


FIG. 2: (Color online) The intensity of the SH components of the patterns displayed in Fig. 1.

the simulations performed, for the same values of W_0 , α , and A , with the “tailless” version of input (3), in which only the main lobe of the Airy-wave profile is kept, while the rest is eliminated. It is seen that the patterns generated by the full AW, and solely by its main lobe, become essentially different with the increase of the number of the generated solitons. Naturally, the patterns originating from the “tailless” inputs feature much weaker radiation components. Nevertheless, the “tailless” initial beam, that keeps the inherent asymmetry of the AW, is basically different from the ordinary symmetric inputs which were commonly used for the downconversion-driven generation of $\chi^{(2)}$ solitons [29]-[31].

It is natural to measure the share of the total power carried by each major soliton generated from the AW input (3). These shares are displayed, as functions of the truncation factor A , in Fig. 3, for the full and “tailless” inputs alike. In particular, in the single-soliton pattern generated by the full input, the share captured by the soliton decreases roughly $\sim 1/\sqrt{A}$ with the growth of A , which implies that only a few leading lobes of the Airy-shaped input build the single soliton, while the total power of the input grows $\sim \sqrt{A}$ [see Eq. (4)]. On the other hand, the combined share carried by all the solitons in the multi-soliton pattern decreases essentially slower, which implies that, as mentioned above, the generation of several solitons is a coherent effect produced by the entire Airy-shaped input.

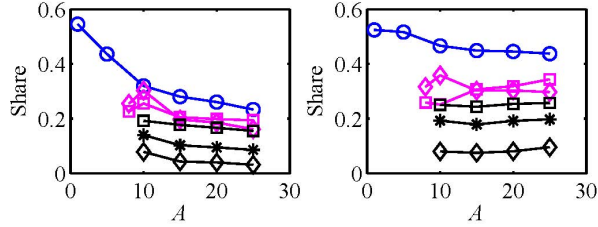


FIG. 3: (Color online) The share of the total power, defined per Eq. (2), which is carried away by each major $\chi^{(2)}$ soliton, vs. the truncation factor, A , of the SH input (3). The number of lines of each color corresponds to the number of major solitons, generated at the same values of W_0 and α for which examples are displayed in Figs. 1 and 2. In the case when more than a single soliton is generated, symbols \square , $*$, and \diamond correspond to the leftmost, middle (in the case of three solitons), and rightmost solitons, respectively. Like in Fig. 1, the left and right panels pertain, severally, to the full and “tailless” inputs.

Naturally, the result of the evolution of the “tailless” input is not sensitive to the overall truncation. At large values of A , the net power share carried away by the one/two or three solitons is larger, respectively, by factors $\simeq 1.8$ or $\simeq 2.2$ in the case of the “tailless” initial conditions, as in that case much less power is spent on the generation the jets and radiation.

Note that, if a single soliton is generated, it always moves to the right, i.e., in the same direction in which the input AW self-accelerates in the framework of the linear equation for the SH. On the other hand, the two- and three-soliton patterns feature, in Figs. 1 and 3, a situation in which a soliton with a larger amplitude may move in the opposite direction, carrying a larger power than that carried to the right by one or two other solitons. As mentioned above, in all cases the total momentum (2) remains equal to zero.

The spatial symmetry of the system suggests to consider a combination of two inputs which launch the self-bending AWs in the opposite directions, with separation $\xi > 0$ and phase shift ϕ between them:

$$w(x, z=0) = W_0 \left[\text{Ai}(\alpha(x + \xi/2)) e^{i\phi/2 + \alpha(x + \xi/2)/A} + \text{Ai}(\alpha(-x + \xi/2)) e^{-i\phi/2 + \alpha(-x + \xi/2)/A} \right]. \quad (5)$$

This input is subject to the Hermitian-symmetry condition, $w(-x, z=0) = w^*(x, z=0)$, which holds in the course of the subsequent evolution. In the absence of the FF seed,

input (5) gives rise to two linear SH waves passing through each other, while the perturbed evolution creates $\chi^{(2)}$ solitons from the left and right AW components, which interact with each other. Here we report results obtained for large values of α , corresponding to relatively small values of P_0 in Eq. (4), i.e., the generation of a single soliton by each AW input separately (otherwise, the interaction pattern is very complex).

Typical results of the interaction of two symmetric AW inputs are presented in Figs. 4 and 5, for both in-phase and out-of-phase pairs, i.e., $\phi = 0$ and $\phi = \pi$ in Eq. (5). When the separation between them is small enough ($\xi \leq 20$ for $\phi = 0$, and $\xi \leq 11$ for $\phi = \pi$), the closely set left and right inputs generate a single soliton, in agreement with the fact that each input carries a value of P_0 which is far too small for the creation of more than one soliton. However, the increase of ξ allows the set of the two AW inputs to generate two solitons. In the case of $\phi = \pi$, it is well known that the two solitons, placed at a moderately large distance, repel each other [32], hence they separate and eventually appear as a pair of solitons moving in directions opposite to those implied by the underlying AWs, as observed in Figs. 4 and 5.

In the case of the in-phase input pair (5), with $\phi = 0$, the direct interaction between the emerging solitons should be attractive, on the contrary to what is observed in the left middle panel of Fig. 4, which features separating solitons. However, it is seen too that the space between the solitons is filled by radiation, the pressure from which may give rise to repulsion [33, 34]. Note that, while the two solitons separate, the radiation forms a relatively strong central “jet”. Additional simulations demonstrate that, at specific values of ξ (e.g., $\xi = 38$ and $\xi = 17$, for $\phi = 0$ and $\phi = \pi$, respectively) the central “jet” may form an additional soliton. Lastly, if ξ is large enough ($\xi \geq 40$ for $\phi = 0$ and $\xi \geq 28$ for $\phi = \pi$), the two AW inputs generate two free solitons, which then collide and merge into a single one, as clearly seen in the bottom row of Fig. 4.

The effect of nonzero mismatch, $q = \pm 1$ in Eq. (1), was explored too. While $q = -1$ prevents the generation of solitons, at the same values of other parameters as considered above, $q = +1$ tends to increase the number of the generated solitons. These trends are easily explained by the cascading approximation, which eliminates the SH in favor of the FF component [29]-[31], $w \approx (2q)^{-1} u^2$, and reduces the $\chi^{(2)}$ system (1) to the single nonlinear Schrödinger equation, $iu_z + (1/2)u_{xx} + (2q)^{-1} |u|^2 u = 0$, which, obviously, gives rise to one or multiple solitons at $q = +1$, and does not produce them at $q = -1$. A typical example

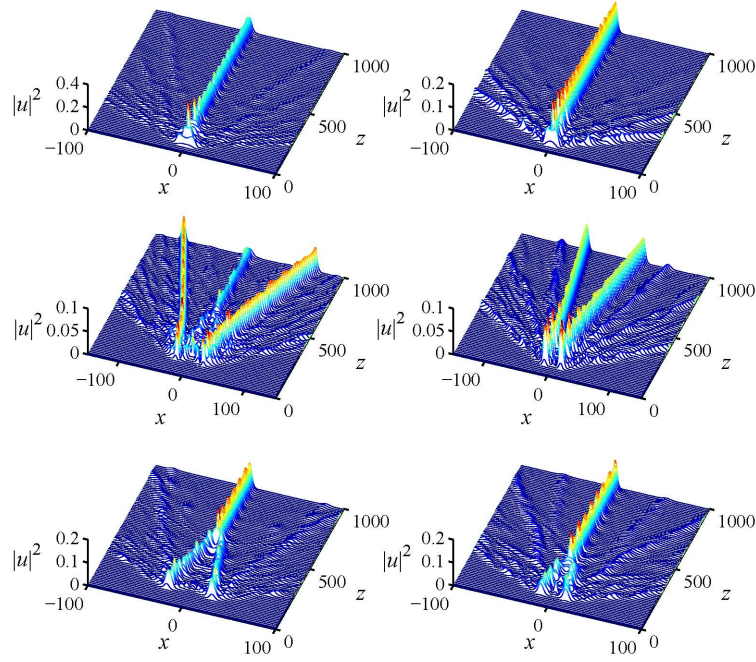


FIG. 4: (Color online) The left and right columns display, severally, the generation of soliton patterns by the in- and out-of-phase pairs of the input AWs in the SH, defined per Eq. (5) with $\phi = 0$ and $\phi = \pi$. The top, middle, and bottom rows demonstrate, respectively, the direct generation of a single $\chi^{(2)}$ soliton (at $\xi = 10$ for both $\phi = 0$ and $\phi = \pi$); the generation of two separating solitons with extra “jets” (at $\xi = 37$ for $\phi = 0$ and $\xi = 20$ for $\phi = \pi$); and the fusion of two emerging solitons into one (at $\xi = 45$ for $\phi = 0$ and $\xi = 23$ for $\phi = \pi$). In all cases, $W_0 = 0.309$, $\alpha = 0.171$, $A = 10$.

of the generation of two solitons at $q = +1$ is displayed in Fig. 6, for parameter values corresponding to $P_0 = 1237$ in Eq. (4), which, as said above, is capable to generate only a single soliton in the system with $q = 0$.

In conclusion, we have proposed a scenario for the interplay of AWs (Airy waves) with the $\chi^{(2)}$ nonlinearity via downconversion, i.e., the PI (parametric instability) seeded by small random FF perturbations added to the truncated AW input in the SH component. Although the downconversion mechanism, driven by the PI, exhibits inherent randomness, it is possible to identify its basic features, such as the number of emerging major solitons and power shares carried by them, including the patterns generated by symmetric pairs of right- and left-bending AW inputs. A natural generalization of the present analysis may be its development for two-dimensional $\chi^{(2)}$ media, where AW inputs are available too, and emerging solitons are stable [30, 31].

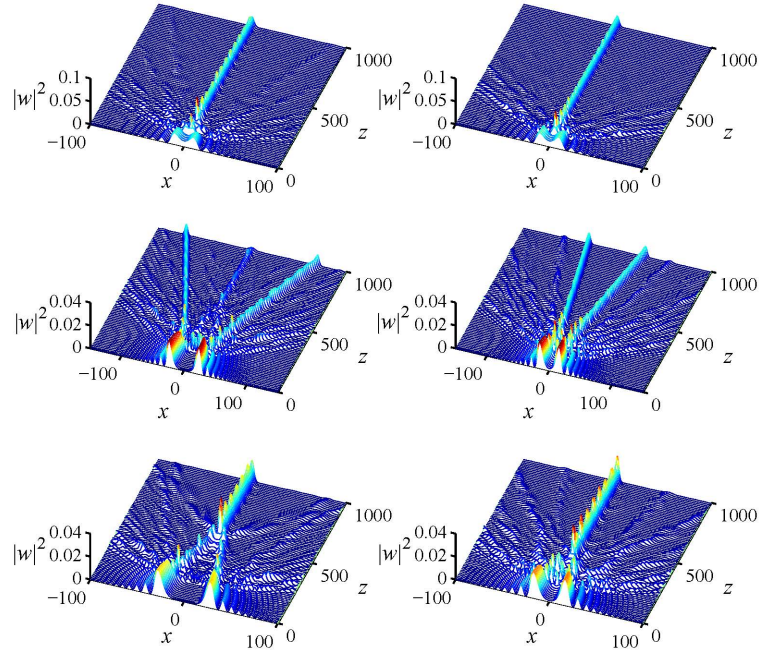


FIG. 5: (Color online) The intensity of the SH components of the patterns displayed in

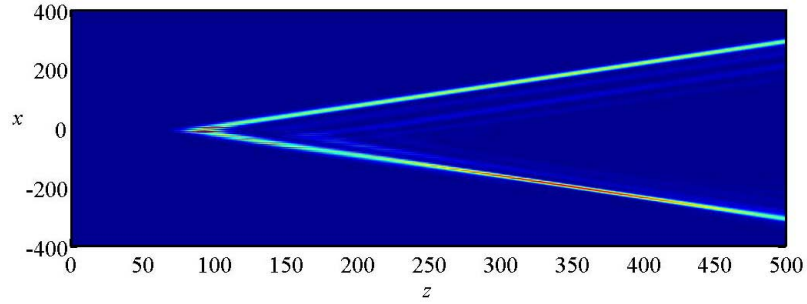


FIG. 6: (Color online) The top view of the generation of two solitons from SH input (3) with $W_0 = 0.2571$, $\alpha = 0.0855$, in the case of mismatch $q = +1$.

Funding Information

Thailand Research Fund (TRF) (RSA5780061).

-
- [1] M. V. Berry and N. L. Balazs, Am. J. Phys. **47**, 264 (1979).
 - [2] G. A. Siviloglou and D. N. Christodoulides, Opt. Lett. **99**, 213901 (2007).
 - [3] G. A. Siviloglou, J. Broky, A. Dogariu, and D. N. Christodoulides, Phys. Rev. Lett. **99**, 213901 (2007).
 - [4] P. Polynkin, M. Kolesik, J. V. Moloney, G. A. Siviloglou, and D. N. Christodoulides, Science

- 324, 229 (2009).
- [5] T. Ellenbogen, N. Voloch-Bloch, A. Ganany-Padowicz, and A. Arie, *Nature Phot.* **3**, 395 (2009).
 - [6] I. Dolev, T. Ellenbogen, and A. Arie, *Opt. Lett.* **35**, 1581 (2010).
 - [7] I. Dolev and A. Arie, *Appl. Phys. Lett.* **97**, 171102 (2010).
 - [8] R. El-Ganainy, K. G. Makris, M. A. Miri, D. N. Christodoulides, and Z. Chen, *Phys. Rev. A* **84**, 023842 (2011).
 - [9] I. Kaminer, M. Segev, and D. N. Christodoulides, *Phys. Rev. Lett.* **106**, 213903 (2011).
 - [10] Y. Fattal, A. Rudnick, and D. M. Marom, *Opt. Exp.* **19**, 17298 (2011).
 - [11] A. Rudnick and D. M. Marom, *Opt. Express*. **19**, 25570 (2011).
 - [12] A. Lotti, D. Faccio, A. Couairon, D. G. Papazoglou, P. Panagiotopoulos, D. Abdollahpour, and S. Tzortzakis, *Phys. Rev. A* **84**, 021807(R) (2011).
 - [13] Y. Hu, Z. Sun, D. Bongiovanni, D. Song, C. Lou, J. Xu, Z. Chen, and R. Morandotti, *Opt. Lett.* **37**, 3201 (2012).
 - [14] I. Dolev, I. Kaminer, A. Shapira, M. Segev, and A. Arie, *Phys. Rev. Lett.* **108**, 113803 (2012).
 - [15] P. Rose, F. Diebel, M. Boguslawski, and C. Denz, *Appl. Phys. Lett.* **102**, 101101 (2013).
 - [16] I. M. Allayarov and E. N. Tsoy, “Dynamics of Airy beams in nonlinear media”, *Phys. Rev. A* **90**, 023852 (2014).
 - [17] R. Driben, Y. Hu, Z. Chen, B. A. Malomed, and R. Morandotti, *Opt. Lett.* **38**, 2499 (2013).
 - [18] Y. Zhang, M. R. Belić, H. Zheng, H. Chen, C. Li, Y. Li, and Y. Zhang, *Opt. Express*. **22**, 7160 (2013).
 - [19] N. K. Efremidis, *Phys. Rev. A* **98**, 023841 (2014).
 - [20] R. Driben, V. V. Konotop, and T. Meier, *Opt. Lett.* **39**, 5523 (2014).
 - [21] C. Ruiz-Jiménez, K. Z. Nóbrega, and M. A. Porras, *Opt. Express*. **23**, 8918 (2015).
 - [22] A. Minovich, A. E. Klein, N. Janunts, T. Pertsch, D. N. Neshev, and Y. S. Kivshar, *Phys. Rev. Lett.* **107**, 116802 (2011).
 - [23] L. Li, T. Li, S. M. Wang, C. Zhang, and S. N. Zhu, *Phys. Rev. Lett.* **107**, 126804 (2011).
 - [24] I. Epstein and A. Arie, *Phys. Rev. Lett.* **112**, 023903 (2014).
 - [25] N. Voloch-Bloch, Y. Lereah, Y. Lilach, A. Gover, and A. Arie, *Nature* **494**, 331 (2013).
 - [26] N. K. Efremidis, V. Paltoglou, and W. von Klitzig, *Phys. Rev. A* **87**, 043637 (2013).
 - [27] M. Clerici, Y. Hu, P. Lassonde, C. Milián, A. Couairon, D. N. Christodoulides, Z. Chen, L.

- Razzari, F. Vidal, F. Légaré, D. Faccio, R. Morandotti, *Sci. Adv.* **1**, e140011 (2015).
- [28] S. Fu, Y. Tsur, J. Zhou, L. Shemer, and A. Arie, *Phys. Rev. Lett.* **115**, 034501 (2015).
 - [29] G. I. Stegeman, D. J. Hagan, and L. Torner, *Opt. Quant. Electron.* **28**, 1691-1740 (1996).
 - [30] C. Etrich, F. Lederer, B. A. Malomed, T. Peschel, and U. Peschel, *Prog. Opt.* **41**, 483 (2000).
 - [31] A. V. Buryak, P. Di Trapani, D. V. Skryabin, and S. Trillo, *Phys. Rep.* **370**, 63 (2002).
 - [32] Y. S. Kivshar and G. P. Agrawal, *Optical Solitons: From Fibers to Photonic Crystals* (Academic Press, San Diego, 2003).
 - [33] R. Driben, A. V. Yulin, A. Efimov, and B. A. Malomed, *Opt. Express.* **21**, 19091 (2013).
 - [34] S. F. Wang, A. Mussot, M. Conforti, X. L. Zeng, and A. Kudlinski, *Opt. Lett.* **40**, 3320 (2015).